Обзор ArXiv: astro-ph, 11-17 сентября 2019

От Сильченко О.К.

ArXiv: 1909.04048

HALOGAS: the properties of extraplanar HI in disc galaxies

A. Marasco[1,2], F. Fraternali[2,3], G. Heald[4], W. J. G. de Blok[1,2,5], T. Oosterloo[1,2], P. Kamphuis[6], G. I. G. Józsa[7,8,9], C. J. Vargas[10], B. Winkel[11], R. A. M. Walterbos[12], R. J. Dettmar[6], and E. Jütte[6]

[1] ASTRON, Netherlands Institute for Radio Astronomy, Oude Hoogeveensedijk 4, 7991 PD, Dwingeloo, The Netherlands
[2] Kapteyn Astronomical Institute, University of Groningen, Postbus 800, 9700 AV, Groningen, The Netherlands
e-mail: marasco@astro.rug.nl
[3] Department of Physics and Astronomy, University of Bologna, via P. Gobetti 93/2, 40129 Bologna, Italy
[4] CSIRO Astronomy and Space Science, PO Box 1130, Bentley WA 6102, Australia
[5] Dept. of Astronomy, Univ. of Cape Town, Private Bag X3, Rondebosch 7701, South Africa
[6] Ruhr-University Bochum, Faculty of Physics and Astronomy, Astronomical Institute, 44780 Bochum, Germany
[7] Department of Physics and Electronics, Rhodes University, PO Box 94, Makhanda, 6140, South Africa
[8] South African Radio Astronomy Observatory, 2 Fir Street, Black River Park, Observatory, Cape Town, 7405, South Africa
[9] Argelander-Institut für Astronomie, Auf dem Hügel 71, D-53121 Bonn, Germany
[10] Department of Astronomy and Steward Observatory, University of Arizona, Tucson, AZ, U.S.A.
[11] Max-Planck-Institut für Radioastronomie, Auf dem Hügel 69, 53121 Bonn, Germany
[12] Department of Astronomy, New Mexico State University, Las Cruces, NM 88001, U.S.A.

Received ; accepted

ABSTRACT

We present a systematic study of the extraplanar gas (EPG) in a sample of 15 nearby late-type galaxies at intermediate inclinations using publicly available, deep interferometric HI data from the HALOGAS survey. For each system we mask the HI emission coming from the regularly rotating disc and use synthetic datacubes to model the leftover 'anomalous' HI flux. Our model consists of a smooth, axisymmetric thick component described by 3 structural and 4 kinematical parameters, which are fit to the data via a Bayesian MCMC approach. We find that extraplanar HI is nearly ubiquitous in disc galaxies, as we fail to detect it in only two of

Выборка из 15 спиральных галактик

Table 1. Physical properties of galaxies in our sample, from H11 and Heald et al. (2012). We also list the median kinematical inclination (INC_{BB}) and position angle (PA_{BB}) found with ^{3D}BAROLO and used in our EPG modelling.

UGC	Other name	Type	dist. (Mpc)	INC_{H11} (°)	INC_{BB} (°)	PA_{BB} (°)	D_{25} (′)	M_B (mag)	v_{rot} ($km\,s^{-1}$)	SFR ($M_\odot\,yr^{-1}$)
1256	NGC 0672	SBcd	7.6	70	67.6	64.2	6.4	-18.65	130.7	0.23
1913	NGC 0925	SABd	9.1	54	57.9	284.7	11.3	-19.66	102.4	0.77
1983	NGC 0949	SAd	11.3	52	52.5	160.8	3.5	-17.85	90.9	0.31
2137	NGC 1003	SAcd	11.6	67	70.4	276.3	6.3	-18.61	95.5	0.40
3918	NGC 2403	SAcd	3.2	62	62.5	124.6	23.8	-19.68	121.9	0.6
4284	NGC 2541	SAcd	12.0	67	63.8	171.8	7.2	-18.37	92.1	0.55[a]
5572	NGC 3198	SBc	14.5	71	70.0	214.3	8.8	-19.62	148.2	1.1
7045	NGC 4062	SAc	16.9	68	67.1	100.1	4.5	-18.27	140.5	0.67
7353	NGC 4258	SABbc	7.6	71	74.0	331.9	17.1	-20.59	208.0	1.7
7377	NGC 4274	SBab	19.4	72	71.3	279.8	6.5	-19.22	239.9	1.2
7539	NGC 4414	SAc	17.8	50	53.9	159.7	4.5	-19.12	224.7	4.2
7591b	NGC 4448	SBab	9.7	71	73.5	94.4	3.8	-18.43	221.6	0.056
7766	NGC 4559	SABcd	7.9	69	68.0	323.1	11.3	-20.07	113.4	0.69
8334	NGC 5055	SAbc	8.5	55	65.2	99.4	13.0	-20.14	215.5	2.1
9179	NGC 5585	SABd	8.7	51	50.4	48.2	5.5	-17.96	79.1	0.41

[a] based on TIR+UV measurements from Thilker et al. (2007) and re-scaled to the distance used in this work. Heald et al. (2012) report only an upper limit based on a non-detection with IRAS 25μm.

Из полного куба данных WSRT вычитается тонкий диск HI

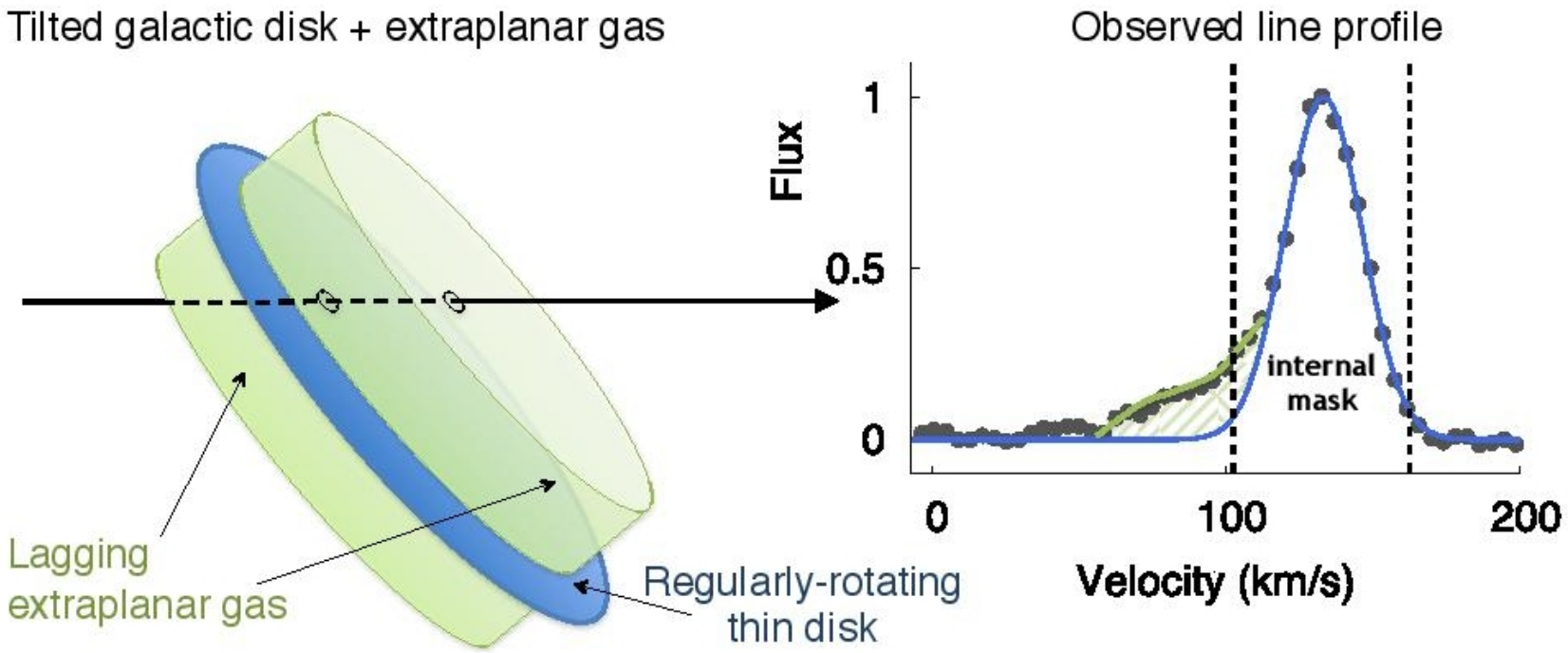

Fig. 1. A sketch of an observation of extraplanar gas in a galaxy seen at intermediate inclination. The typical line profile (along the kinematic major axis of the galaxy) will be composed by a nearly Gaussian part coming from the thin disc with overlaid a tail at low rotation velocity produced by the lagging EPG layer. The width of the disc emission is roughly symmetrical, produced by gas turbulence and well fitted by a Gaussian function (blue solid line). The EPG separation is achieved by masking a portion of the profile with substantial contribution from this Gaussian function ('internal mask' region).

К тому, что осталось, применяют модель толстого диска:

$$\Sigma(R) = \Sigma_0 \left(1 + \frac{R}{R_g}\right)^{\gamma} \exp\left(-\frac{R}{R_g}\right),$$

$$\rho(z) \propto \frac{\sinh(|z|/h)}{\cosh^2(|z|/h)},$$

3 структурных параметра, и 4 - кинематических

The EPG kinematics is described by four parameters: the vertical gradient in the gas rotational speed (dv_ϕ/dz), the velocities in the radial and in the vertical directions (v_R and v_z), and gas velocity dispersion σ. Thus the EPG is allowed to rotate with a different speed with respect to the material within the disc (or to not rotate at all, for $dv_\phi/dz \ll 0$). It can globally accrete onto or escape from the galaxy, can move in/out and have a different velocity dispersion. These simple kinematical parameters allow us

Индивидуальные результаты:

Table 4. Best-fit parameters and associated uncertainty for the EPG of the galaxies studied in this work.

Galaxy	Beam	Independent	$M_{\rm HI,EPG}$	$f_{\rm EPG}$	$R_{\rm g}$	γ	h	$\mathrm{d}v_\phi/\mathrm{d}z$	v_R	v_z	σ
	(arcsec)	voxels	(10^8 M$_\odot$)		(kpc)		(kpc)	(km s^{-1} kpc^{-1})	(km s^{-1})	(km s^{-1})	(km s^{-1})
(1)	(2)	(3)	(4)	(5)	(6)	(7)	(8)	(9)	(10)	(11)	(12)
NGC 0672[a]	42x32	936	4.9	0.14	6.3±0.4	0.1±0.1	1.5±0.1	-8.4±0.5	-25.8±1.4	-35.4±2.4	25.3±0.9
NGC 0925[a]	38x33	870	7.6	0.14	0.9±0.1	13.3±2.1	2.0±0.1	-9.7±0.7	3.3±3.5	-17.8±5.6	21.6±1.3
NGC 0949	39x35	190	1.6	0.27	3.9±0.8	0.5±0.5	1.6±0.1	-18.0±1.4	-29.6±3.5	-19.1±3.5	27.7±1.6
NGC 2403	30x29	4797	5.9	0.22	2.3±0.1	2.6±0.3	0.9±0.1	-11.7±0.5	-21±0.9	-9.4±1.2	15.2±0.4
NGC 2541	34x34	634	7.4	0.15	-	4.9±1.0	2.8±0.1	-6.5±0.3	-24.3±1.9	-15.9±2.3	27.4±1.0
NGC 3198	35x33	637	9.8	0.09	2.1±0.5	9.8±2.8	1.4±0.2	-9.2±1.4	-1.5±2.6	8.1±8.9	23.0±1.2
NGC 4062	39x34	148	2.1	0.11	-	5.0±2.2	2.5±0.1	-9.4±1.0	-25.8±5.8	-23±7.5	34.6±2.0
NGC 4258	33x33	1422	6.6	0.11	6.6±1.1	2.3±0.4	1.4±0.1	-10.0±0.5	-17.3±1.3	-27.2±3.8	24.8±0.7
NGC 4414[b]	39x33	194	5.1	0.12	-	-3.7±1.9	0.5±0.3	-58^{+24}_{-56}	-39.5±4.8	-13.1±14.2	26.3±2.9
NGC 4559	41x32	926	6.0	0.13	1.9±0.3	4.0±0.9	1.7±0.1	-8.2±0.6	-19.8±2.5	-33.9±4.1	21.3±1.2
NGC 5055[b]	36x33	491	2.6	0.04	1.1±0.2	8.3±1.5	0.6±0.1	-40^{+8}_{-13}	-13.7±3.9	-39.5±8.6	20.2±2.4
NGC 5585	34x33	368	3.0	0.12	$2.5^{+1.9}_{-0.9}$	2.6±1.8	1.4±0.3	-2.3±0.8	0.4±2.4	5.4±4.0	18.5±1.0

Notes. (1) NGC name; (2) FWHM of the synthesised beam; (3) Number of independent EPG voxels modelled, computed as the number of voxels in the masked dataset with intensity above twice the rms-noise divided by the number of voxels per resolution element (eq. 6); (4) H I mass of the EPG component, with an uncertainty of ~ 20%; (5) ratio between $M_{\rm EPG}$ and the total H I mass; (6-7) surface density parameters (eq. 1), a '-' indicates that the parameter is unconstrained; (8) scale height (eq. 2); (9) vertical rotational gradient; (10) velocity in the direction perpendicular to the rotational axis (positive values mean outflow); (11) velocity in the direction perpendicular to the disc (positive values mean outflow); (12) velocity dispersion.

[a] Interacting systems.

[b] Poorly-fit systems, which are also warped. The fit is limited to (and $f_{\rm EPG}$ is computed within) the innermost 20 kpc.

В основном, аккреция: радиальная и вертикальная

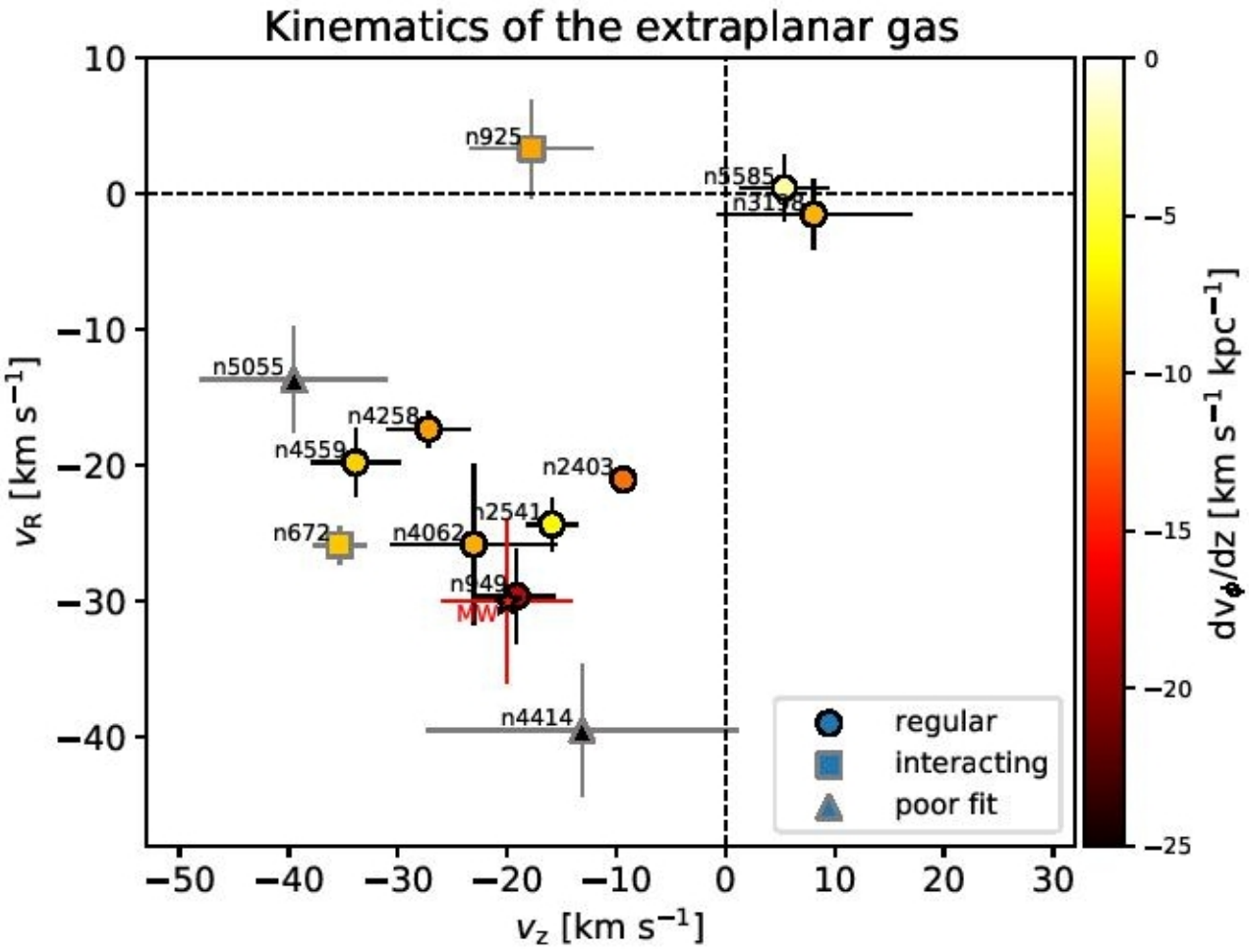

Происхождение толстого диска HI: «Фонтанное»

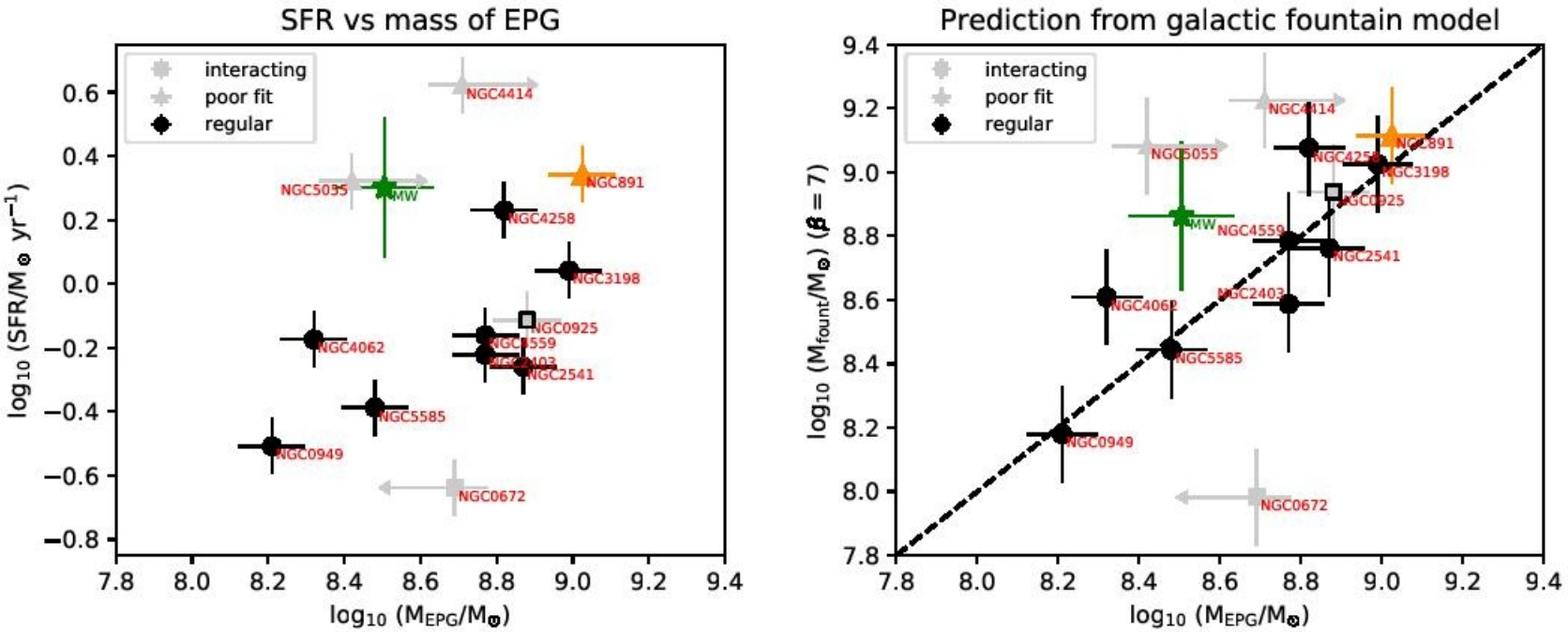

Fig. 11. *Left panel*: SFR vs EPG mass for our HALOGAS sample. *Right panel*: theoretical EPG mass predicted by a galactic fountain model (eq. 11 with $\beta = 7$) vs that inferred from the data. The two panels span the same range ($\sim$ 1.5 dex) on both axes. Error-bars are determined by assuming a 10% uncertainty on the distances and a 20% uncertainty on the total SFR, in addition to the uncertainty on the R_{SFR} discussed in the text. Interacting galaxies and systems with a poorly fit EPG are shown with separate symbols. We have also included NGC 891(M_{EPG} from Marinacci et al. 2010b) and the Milky Way, for which we used $M_{EPG} = 3.2 \pm 1.0 \times 10^8$ $M_\odot$ (MF11), and assumed fiducial values for SFR, R_{SFR} and v_{flat} of 2 ± 1 $M_\odot$ yr^{-1}, 2.5 ± 0.5 kpc and 240 ± 10 km s^{-1} respectively.

ArXiv: 1909.06712

A measurement of the Hubble constant from angular diameter distances to two gravitational lenses

Inh Jee,[1*] Sherry H. Suyu,[1,2,3*] Eiichiro Komatsu,[1,4]
Christopher D. Fassnacht,[5] Stefan Hilbert,[6,7] Léon V. E. Koopmans[8]

Резюме

The local expansion rate of the Universe is parametrized by the Hubble constant, H_0, the ratio between recession velocity and distance. Different techniques lead to inconsistent estimates of H_0. Observations of Type Ia supernovae (SNe) can be used to measure H_0, but this requires an external calibrator to convert relative distances to absolute ones. We use the angular diameter distance to strong gravitational lenses as a suitable calibrator, which is only weakly sensitive to cosmological assumptions. We determine the angular diameter distances to two gravitational lenses, 810^{+160}_{-130} and 1230^{+180}_{-150} Mpc, at redshifts of $z = 0.295$ and 0.6304. Using these absolute distances to calibrate 740 previously-measured relative distances to SNe, we measure the Hubble constant to be $H_0 = 82.4^{+8.4}_{-8.3}\,\mathrm{km\,s^{-1}\,Mpc^{-1}}$.

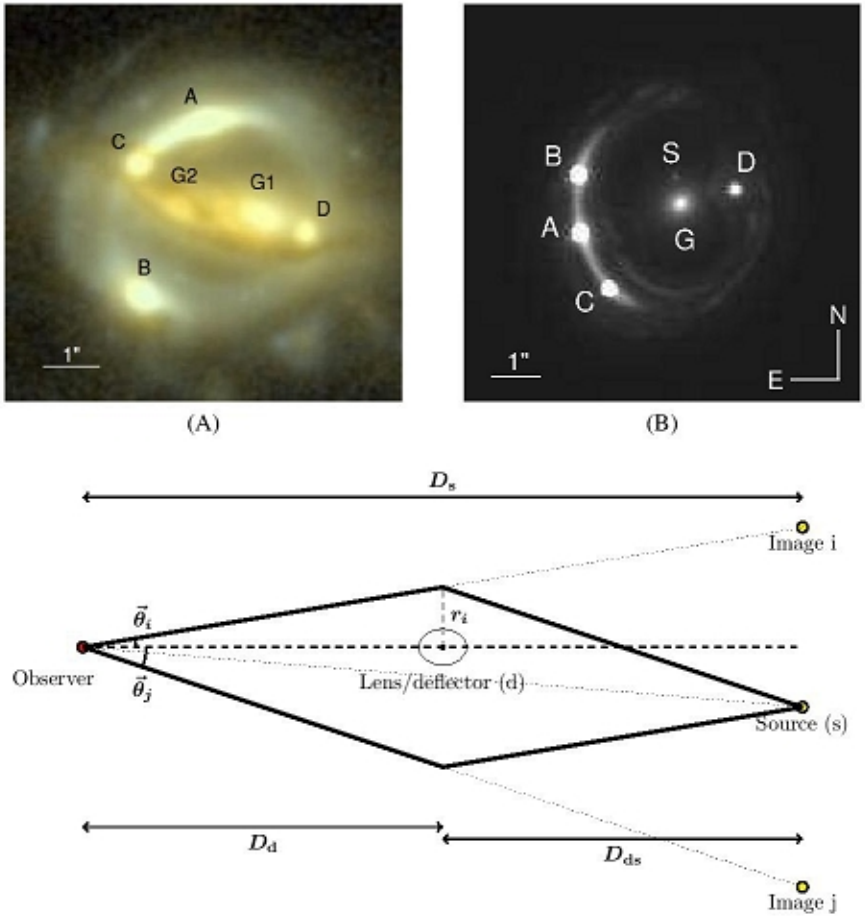

posite image of lens B1 8+656 (A) and ACS F814W image of RXJ1131−1231 (B) (*17,18,22*).
Labels A-D are the quasar images, G (1-2) are lens galaxies, and S is a satellite galaxy. (C)

3 измеряемых величины:
угловое расстояние между изображениями
задержка переменности,
дисперсия скоростей звезд в линзе.

Включение в модель кинематики звезд в линзе очень улучшает точность

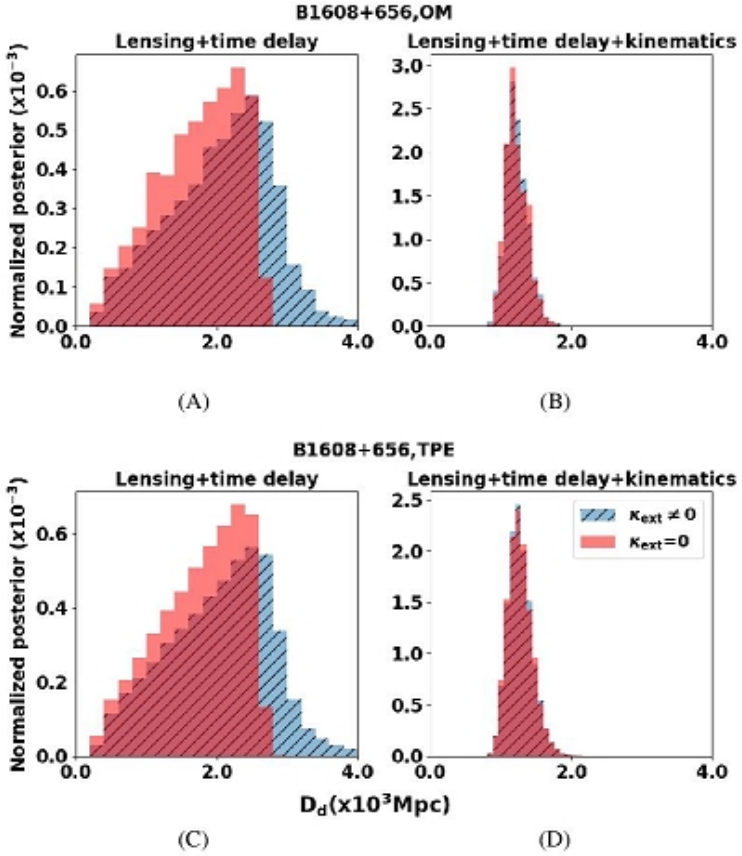

Figure 3: **Normalized posterior probability distributions for the angular diameter distance to the lens B1608+656.** (A, C) include lensing and time-delay information, while (B, D) include additionally the kinematics of the lens. The blue hatched distribution shows the results if the external convergence distribution is estimated by ray-tracing through the Millennium Simulation (*36*) (Fig. S4), while the red distribution is the result when the external convergence is set to zero. By including the kinematic information, the angular diameter distance becomes insensitive to κ_{ext}.

Измеренные расстояния до галактик-линз и их использование для калибровки SNI

Our analysis constrains the angular diameter distances to 12–20% precision per lens. We marginalize over the uncertainties in anisotropy models by merging two posterior probability distributions of OM and TPE models (Section S6). Our final measurements of the angular diameter distances are $D_{\rm d}(z = 0.6304) = (1.23^{+0.18}_{-0.15}) \times 10^3$ Mpc for B1608+656, and $D_{\rm d}(z = 0.295) = (8.1^{+1.6}_{-1.2}) \times 10^2$ Mpc for RXJ1131−1231.

We apply these distances as anchors to the 740 SNe in the Joint Light-curve Analysis (JLA, (*37*)) dataset, allowing us to constrain H_0 and the SNe nuisance parameters (Section S7) simultaneously. We use the MontePython code (*38*) to perform a Markov Chain Monte Carlo analysis. Fig. 5 shows the resulting Hubble diagram, i.e. the absolute luminosity distances $D_{\rm L} = (1 + z)^2 D_{\rm d}$ as a function of redshifts for a flat ΛCDM model.

Откалиброванная диаграмма Хаббла для сверхновых

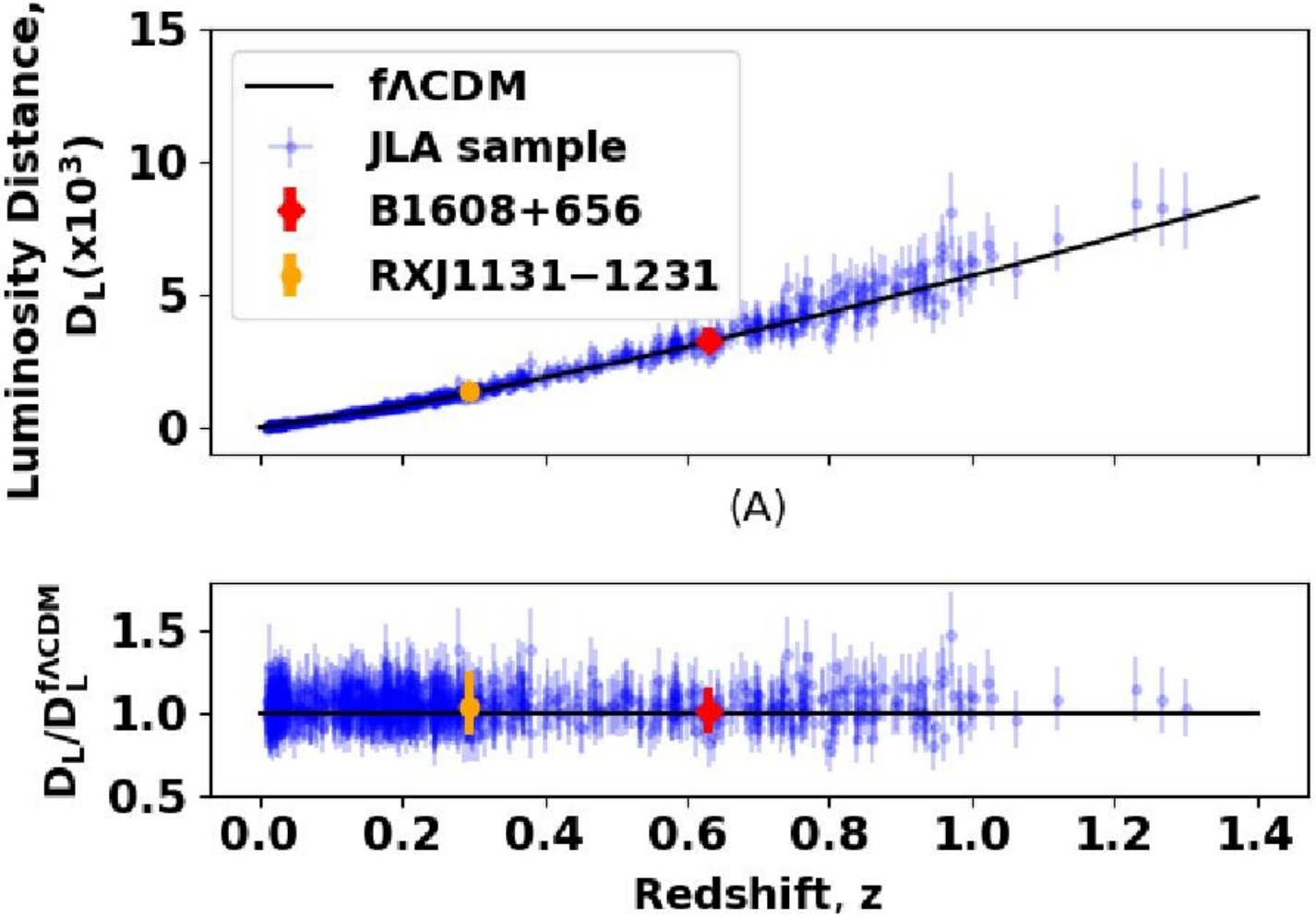

Полученная из нее постоянная Хаббла

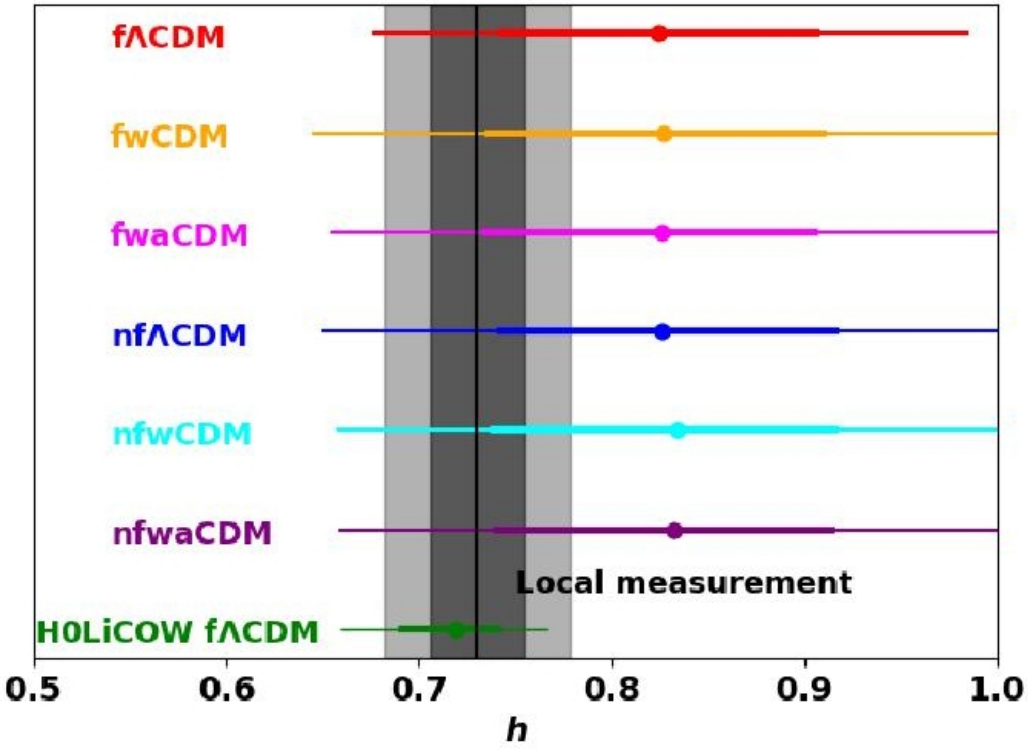

Figure 6: **Constraints on the Hubble constant for six cosmological models.** The gray shaded area is the constraint from the local distance ladder (*4*), while the green line is from three time-delay distances measured by the H0LiCOW collaboration (*24*). The thick and thin solid lines denote the 68% and 95% Confidence Levels of the joint fit to the SNe and the $D_{\rm d}$ data. We emphasize that $D_{\rm d}$ and $D_{\Delta t}$ determined from the same lens are not correlated strongly because the uncertainty in the former is dominated by the kinematics and the latter by $\kappa_{\rm ext}$ in the case of